

# **Modeling transient Groundwater Flow for Stability Assessment of Dikes**

dr.ir. J.M. van Esch

1206015-003



**Title**

Modeling transient Groundwater Flow for Stability Assessment of Dikes

**Client**

Rijkswaterstaat

**Project**

1206015-003

**Reference**

1206015-003-GEO-0001

**Pages**

25


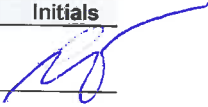
**Keywords**

Groundwater, dikes, consolidation, finite elements

**Summary**

Dikes and levees protect the land from flooding by retaining high water levels. However, water penetrating the dike and the subsoil during high water periods reduces the strength of the dike due to the increase in pore pressure. Moreover, the raise in hydraulic head in deeper layers may lead to uplift of the top layer at the polder side of the dike, and finally an increase in potential head might lead to an internal erosion process called piping. To assess these effects it is important to have an adequate knowledge of the pore water pressure field.

Nowadays pore water pressure fields are often obtained by solving the storage equation. This approach provides a computationally efficient method and requires less soil parameters than needed for solving the fully coupled flow-deformation problem. However, the storage equation is not able to simulate the generation of pore water pressure due to hydraulic loading of the subsurface correctly. This paper presents a numerical model for solving Biot's problem and compares the solution of its flow-deformation formulation to the solution of the storage equation. Future work should indicate for which cases the generation of pore water pressures should be included in modeling transient groundwater flow for stability assessment. Future work should also consider the applicability of the heuristic loading procedure already included in Fewes-Dam.

| Version | Date      | Author               | Initials | Review                  | Initials   | Approval     | Initials  |
|---------|-----------|----------------------|----------|-------------------------|--|--------------|---|
| 1       | dec. 2012 | dr.ir. J.M. van Esch |          | dr.ir. J.A.M. Teunissen |  | Ir. L. Voogt |  |
|         |           |                      |          |                         |  |              |   |
|         |           |                      |          |                         |  |              |   |

**State**

preliminary

This is a preliminary report, intended for discussion purposes only. No part of this report may be relied upon by either principal or third parties.



## Contents

|                                |           |
|--------------------------------|-----------|
| <b>1 Introduction</b>          | <b>1</b>  |
| <b>2 Mathematical model</b>    | <b>5</b>  |
| 2.1 Equilibrium equation       | 5         |
| 2.2 Storage equation           | 6         |
| 2.3 Governing equation         | 8         |
| <b>3 Numerical model</b>       | <b>11</b> |
| 3.1 Numerical formulation      | 11        |
| 3.2 Algebraic equations        | 13        |
| <b>4 Numerical experiments</b> | <b>15</b> |
| 4.1 Undrained loading          | 15        |
| 4.2 Drained loading            | 17        |
| 4.3 Hydraulic loading          | 18        |
| <b>5 Conclusions</b>           | <b>21</b> |
| <b>Notations</b>               | <b>23</b> |
| <b>Bibliography</b>            | <b>25</b> |



## List of Tables

|           |                                   |    |
|-----------|-----------------------------------|----|
| Table 4.1 | external material parameters..... | 15 |
|-----------|-----------------------------------|----|





## List of Figures

|            |   |    |
|------------|---|----|
| Figure 1.1 | Piezolines in a dike geometry.....                            | 1  |
| Figure 1.2 | Flow versus flow-deformation simulation. ....                 | 2  |
| Figure 1.3 | Piezometric heads in a Watex geometry.....                    | 2  |
| Figure 4.1 | Numerical and closed form solution for undrained loading..... | 16 |
| Figure 4.2 | Undrained loading presided by gravity loading .....           | 17 |
| Figure 4.3 | Drained loading. ....   | 18 |
| Figure 4.4 | Hydraulic loading. ....                                       | 19 |
| Figure 5.1 | Finite element mesh flow-deformation problem.....             | 22 |



## 1 Introduction

This report considers transient groundwater flow for stability assessment of dikes and presents a numerical model for solving Biot's problem that considers pore water pressures and displacement of the soil. The numerical code is added to the Deltares groundwater flow module DgFlow [6], which supports the dike analysis module DAM [4, 5] of the flood early warning system FEWS. Delft-FEWS [9] is acknowledged worldwide for the real time forecasting of hydrodynamic water levels and waves in rivers, lakes and seas, using prediction models and monitoring data.

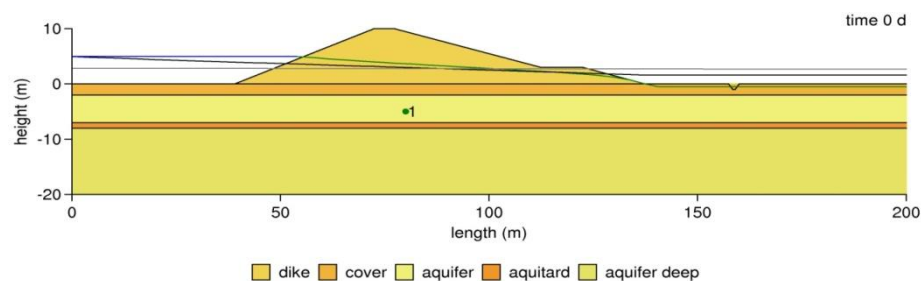


Figure 1.1 Piezolines in a dike geometry.

Groundwater flow simulations provide predictions of the water pressure field in the dike, which can be used for the stability assessment. The finite element method is often preferred for solving these problems because of the flexibility of this technique in capturing complex geometries [2]. Figure 1.1 illustrates the outcome of a simulation for a system of two aquifers confined by aquitards and a dike. The figure shows the piezolines in the aquifer and the embankment. Piezolines follow from an averaging procedure in vertical direction over an aquifer for which they hold. The groundwater simulations presented in this report give a two-dimensional water pressure field that can be used for stability analysis directly. The difference between the total stress and water pressure gives the effective stress, which relates to the shear stress and slope stability.

The blue line displays the free water level at the river side, and the green line presents the phreatic surface in the dike. The phreatic surface resembles the pressure contour that has a zero value. In this configuration seepage occurs at the lower end of the berm, where the green line intersects the dike surface. The black line presents the decline of the hydraulic head in the aquifer from the river side to the polder.

Nowadays pore water fields follow from solving the storage equation. This procedure provides a computational efficient method and requires less soil parameters than for solving Biot's problem. The Biot model couples the storage equation to the equilibrium equation and is able to simulate the generation and dissipation process. The storage equation by itself is not able to simulate the generation of pore water pressure due to hydraulic loading and compression of the subsurface. Figure 1.2 shows the results of an oedometer test simulation loaded by an increasing water level at the top. The left picture shows the water pressure generation as simulated by solving the storage equation, the right picture follows from solving the fully coupled storage-equilibrium equation.

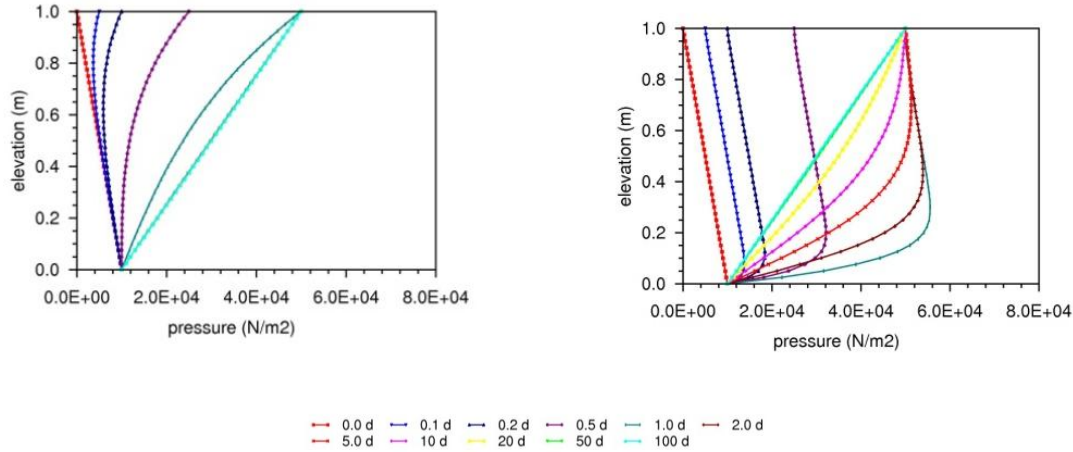


Figure 1.2 Flow versus flow-deformation simulation.

Watex solves the transient flow equation in quasi two dimensionally and adds a pore water generation procedure to simulate the effect of hydraulic loading. Figure 1.3 presents a simplified geometry for which the procedure will be outlined.

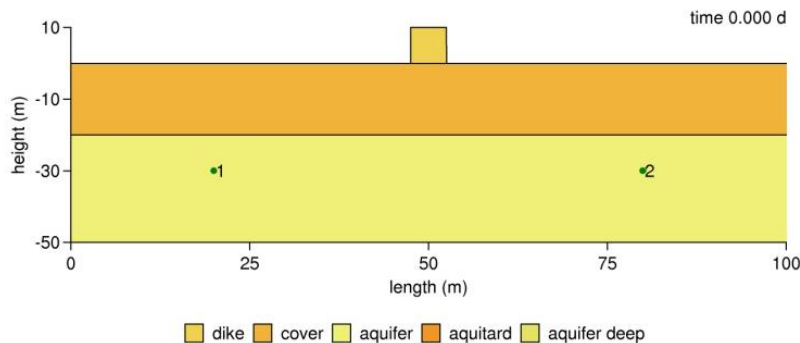


Figure 1.3 Piezometric heads in a Watex geometry.

The flow equation is solved in the flow domain denoted by  $\Omega$  ( $m^2$ ), the boundary of which will be denoted by  $\Gamma$  ( $m$ ). The independent variables are time  $t$  (s) and space  $(x, y)$  ( $m$ ), the primary unknown is hydraulic head  $\phi$  ( $m$ ). The flow equation is given by

$$\rho g (\alpha + n\beta) \frac{\partial \phi}{\partial t} = k_{xx} \frac{\partial^2 \phi}{\partial x^2} + k_{yy} \frac{\partial^2 \phi}{\partial y^2} \quad \text{on } \Omega \quad (1.1)$$

where  $\rho$  ( $kg/m^3$ ) denotes the density of the pore water,  $g$  ( $m/s^2$ ) is gravity,  $\alpha$  ( $m^2/N$ ) is the compressibility of the soil,  $n$  (-) expresses porosity of the porous medium,  $\beta$  ( $m^2/N$ ) is the compressibility of the pore water holding gas inclusions,  $k_{xx}$  and  $k_{yy}$  ( $m/s$ ) denote hydraulic conductivity in both spatial directions. On the boundary conditions apply that close

the flow equation. Dirichlet boundary conditions simulate the river level in time  $h(t)$  (m) at the left side of the construction and a constant Dirichlet condition simulates the polder water level at the right side. These condition close the flow equation (1.1) by

$$\phi = h(t) \quad \text{on} \quad \Gamma_r, \quad \phi = c \quad \text{on} \quad \Gamma_p \quad (1.2)$$

Von Neumann or second-type boundary conditions prescribe the derivative of the head or zero flux on the remaining boundary.

Hydraulic head follows from the pore pressure  $p$  ( $\text{N/m}^2$ ) as  $\phi = p / \rho g + y$ . The proposed flow model is not able to simulate the fully coupled water phase - soil phase behavior because the equilibrium equation, describing the deformation of the soil skeleton, is omitted. Loading of the water phase underneath the river bed by water level changes is taken into account in a heuristic manner. According to this approach, the load increment  $\delta\sigma$  ( $\text{N/m}^2$ ) distributes over the liquid phase  $\delta p$  ( $\text{N/m}^2$ ) and the soil skeleton  $\delta\sigma'$  ( $\text{N/m}^2$ ) according to

$$\delta p = \frac{\alpha}{\alpha + n\beta} \delta\sigma \quad \delta\sigma' = \frac{n\beta}{\alpha + n\beta} \delta\sigma \quad (1.3)$$

For each time step, the hydraulic head obtained in the previous time step is adjusted as  $\phi^{n*} = \phi^n + \alpha\Delta h / (\alpha + n\beta)$ , where  $\Delta h$  is the water level increase over the time step.

Chapter 2 presents the mathematical flow-deformation model. The fully coupled equilibrium equation and storage equation forms Biot's model, which provides the governing equation. Chapter 3 gives the numerical model. First the numerical formulation will be presented, and then the resulting set of algebraic equations and the numerical solution procedure will be outlined. Chapter 4 provides a set of numerical experiments; undrained loading, drained loading and hydraulic loading of an oedometer test. Chapter 5 draws the conclusions and presents recommendations for future work. This future work should consider the applicability of a heuristic loading procedure already available in Few's-Dam.



## 2 Mathematical model

The small deformation formulation is based on the small strain theory. The coupled set of equilibrium equation and storage equation forms Biot's model [7,8]. The equilibrium equation [1] follows from conservation of moment of momentum, balance of momentum, Terzaghi's effective stress formulation, Hooke's generalized linear elastic constitutive law, and the strain-displacement equation. The storage equation [2, 3] follows from the mass balance equation and Darcy's empirical law. Throughout this report compressive stresses are positive, and saturated pore pressures are positive. In the first and second section index notation will be used,  $x_i$  denotes Cartesian coordinates in space and  $t$  denotes time,  $\Omega$  ( $m^2$ ) represents the deformation-flow domain and  $\Gamma$  ( $m$ ) its boundary. The third section adopts the matrix-vector notation, which facilitates effective coding and maps the fourth order material stiffness tensor on a simple matrix.

### 2.1 Equilibrium equation

The momentum balance equation reads

$$\frac{\partial \sigma_{ij}}{\partial x_j} - \rho g_i = 0 \quad \text{on } \Omega \quad (2.1)$$

where  $\sigma_{ij}$  ( $N/m^2$ ) denotes the total Cauchy stress,  $\rho$  is the soil density ( $kg/m^3$ ), and  $g_i$  represents the gravitational acceleration vector ( $m/s^2$ ). For a y-coordinate pointing in opposite direction of the gravitational vector  $g_y = -9.81 m/s^2$ . The soil density follows from the solid phase density and the liquid phase density as  $\rho = (1-n)\rho^s + n\rho^l$ , where  $n$  (-) is the porosity of the soil. Conservation of moment of momentum requires

$$\sigma_{ij} = \sigma_{ji} \quad (2.2)$$

Terzaghi's principle states that the total stress follows from the effective stress  $\sigma'_{ij}$  ( $N/m^2$ ) and the pore pressure  $p$  ( $N/m^2$ ). This effective stress principle is written as

$$\sigma_{ij} = \sigma'_{ij} + pS\delta_{ij} \quad (2.3)$$

In this expression  $\delta_{ij}$  (-) denotes the Kronecker delta and  $S$  (-) is saturation, which represents the part of the pore space that is filled with pore water. The constitutive equation relates the effective stress to the stain and states for an elastic material

$$\sigma'_{ij} = -D_{ijkl}\epsilon_{kl} \quad (2.4)$$

Here  $D_{ijkl}$  ( $\text{N/m}^2$ ) denotes the fourth order material stiffness tensor and  $\epsilon_{kl}$  (-) is the second order strain tensor. The material stiffness tensor formulated in Lamé constants  $\lambda$  ( $\text{N/m}^2$ ) and  $\mu$  ( $\text{N/m}^2$ ) reads

$$D_{ijkl} = \mu (\delta_{ik} \delta_{jl} + \delta_{il} \delta_{jk}) + \lambda \delta_{ij} \delta_{kl} \quad (2.5)$$

The strain-displacement expression relates displacement  $u_i$  (m) to strain according to

$$\epsilon_{ij} = \frac{1}{2} \left( \frac{\partial u_i}{\partial x_j} + \frac{\partial u_j}{\partial x_i} \right) \quad (2.6)$$

The equilibrium equation now follows from equations (2.1), (2.2), (2.3), (2.4), (2.5) and (2.6) as

$$\frac{1}{2} \frac{\partial}{\partial x_j} \left[ D_{ijkl} \left( \frac{\partial u_k}{\partial x_l} + \frac{\partial u_l}{\partial x_k} \right) \right] - \frac{\partial}{\partial x_i} (pS) + \rho g_i = 0 \quad \text{on } \Omega \quad (2.7)$$

In this report two types of boundary conditions that close the equilibrium equation (2.7) will be discussed. Dirichlet boundary conditions prescribe the displacement according to

$$u_i = \bar{u}_i \quad \text{on } \Gamma_1^u \quad (2.8)$$

and Cauchy boundary conditions specify a boundary force as

$$\sigma_{ij} n_j = \bar{\tau}_i \quad \text{on } \Gamma_2^u \quad (2.9)$$

In the definition of the boundary conditions  $\Gamma_1^u$  (m) and  $\Gamma_2^u$  (m) denote disjoint parts of the deformation boundary,  $\bar{u}_i$  (m) expresses the prescribed displacement and  $\bar{\tau}_i$  ( $\text{N/m}^2$ ) is the imposed boundary compressive force vector. The normal unit vector  $n_i$  (-) points into the domain.

## 2.2 Storage equation

The mass balance equation for the liquid phase reads

$$\frac{\partial}{\partial t} (nS \rho^l) + \frac{\partial}{\partial x_i} (nS \rho^l v_i) = 0 \quad \text{on } \Omega \quad (2.10)$$

where  $v_i$  (m/s) is the average velocity of the fluid. The density of the liquid phase is assumed to depend on the liquid phase pressure by an equation of state that reads  $\rho^l = \rho_0^l \exp[\beta(p - p_0)]$ , where  $\beta$  ( $\text{m}^2/\text{N}$ ) is the compressibility of the fluid and  $\rho_0$



( $\text{kg/m}^3$ ) expresses the density of the fluid at reference pressure  $p_0$  ( $\text{N/m}^2$ ). Using this expression, conservation of mass of the fluid can be written as

$$\frac{\partial nS}{\partial t} + n\beta \frac{\partial p}{\partial t} + \frac{\partial}{\partial x_i}(nSv_i) = 0 \quad \text{on } \Omega \quad (2.11)$$

The mass balance equation for the solid phase reads

$$\frac{\partial}{\partial t}[(1-n)\rho^s] + \frac{\partial}{\partial x_i}[(1-n)\rho^s w_i] = 0 \quad \text{on } \Omega \quad (2.12)$$

where  $w_i$  (m/s) is the velocity of the solid phase. Under the assumption that the density of the solids is constant, this equation can be rewritten as

$$-\frac{\partial n}{\partial t} + \frac{\partial}{\partial x_i}[(1-n)w_i] = 0 \quad \text{on } \Omega \quad (2.13)$$

Adding equation (2.11) and equation (2.13) multiplied by saturation eliminates the time derivative of porosity and gives

$$\left(n\beta + n \frac{dS}{dp}\right) \frac{\partial p}{\partial t} + \frac{\partial}{\partial x_i}[nS(v_i - w_i)] + \frac{\partial}{\partial x_i}(Sw_i) = 0 \quad \text{on } \Omega \quad (2.14)$$

where  $\partial w_i / \partial x_i = \partial \epsilon_v / \partial t$  and the volumetric strain  $\epsilon_v$  (-) reads  $\epsilon_v = \partial u_i / \partial x_i$ . The specific discharge  $q_i$  (m/s) expresses the velocity of the fluid phase relative to the velocity of the solid phase as  $q_i = nS(v_i - w_i)$ . Using these relations, equation (2.14) can be reformulated as

$$S \frac{\partial \epsilon_v}{\partial t} + \left(n\beta + n \frac{dS}{dp}\right) \frac{\partial p}{\partial t} + \frac{\partial q_i}{\partial x_i} = 0 \quad \text{on } \Omega \quad (2.15)$$

Darcy's law for fluid motion gives an expression for the specific discharge that reads

$$q_i = -\frac{k_r \kappa_{ij}}{\mu^l} \left( \frac{\partial p}{\partial x_j} - \rho^l g_j \right) \quad (2.16)$$

Here  $\kappa_{ij}$  ( $\text{m}^2$ ) denotes the intrinsic permeability tensor,  $\mu^l$  ( $\text{kg/ms}$ ) is the dynamic viscosity of the liquid phase and  $k_r$  (-) denotes the relative permeability that scales the intrinsic permeability in the unsaturated zone. Hydraulic conductivity  $k_{ij}$  (m/s) follows from intrinsic

permeability as  $k_{ij} = \rho^l g \kappa_{ij} / \mu^l$ . The storage equation for saturated groundwater flow now follows from the mass balance equation (2.15) and Darcy's relation (2.16) and reads

$$S \frac{\partial \epsilon_v}{\partial t} + \left( n\beta + n \frac{dS}{dp} \right) \frac{\partial p}{\partial t} = \frac{\partial}{\partial x_i} \left[ \frac{k_r \kappa_{ij}}{\mu} \left( \frac{\partial p}{\partial x_j} - \rho^l g_j \right) \right] \quad \text{on } \Omega \quad (2.17)$$

Two types of boundary conditions that close storage equation (2.17) will be presented. Dirichlet boundary conditions prescribe the pressure  $\bar{p}$  (N/m<sup>2</sup>) and read

$$p = \bar{p} \quad \text{on } \Gamma_1^p \quad (2.18)$$

and Neumann boundary conditions impose a volume flux  $\bar{q}_n$  (m/s) by

$$q_i n_i = \bar{q}_n \quad \text{on } \Gamma_2^p \quad (2.19)$$

Here the normal unit vector  $n_i$  (-) points into the flow domain  $\Omega$  (m<sup>2</sup>) over a part of the flow boundary  $\Gamma^p$  (m).

## 2.3 Governing equation

The equilibrium equation and the storage equation will be reformulated in plain strain matrix-vector notation, which facilitates effective coding. The primary unknowns will be written as  $[u_x, u_y]^T$  and  $p$  and the formulation will be limited to saturated conditions. First the differential operator  $[\nabla]$  (1/m) and its counterpart  $[L]$  (1/m) will be presented in matrix form as

$$[\nabla] = \begin{bmatrix} \frac{\partial}{\partial x} \\ \frac{\partial}{\partial y} \end{bmatrix}, \quad [L] = \begin{bmatrix} \frac{\partial}{\partial x} & 0 & 0 \\ 0 & \frac{\partial}{\partial y} & 0 \\ 0 & 0 & \frac{\partial}{\partial z} \\ \frac{\partial}{\partial x} & \frac{\partial}{\partial y} & 0 \end{bmatrix} \quad (2.20)$$

The equilibrium equation (2.7) written in matrix form then reads

$$[L]^T [\sigma] - \rho [g] = [0], \quad [\sigma] = -[D][L][u] + p[m] \quad (2.21)$$

where the stress mapping column reads  $[m] = [1110]^T$  and  $[g] = [0 -9.81]^T$  if the gravitation vector point in negative  $y$ -direction. The engineering strain vector  $[\epsilon] = [\epsilon_{xx} \ \epsilon_{yy} \ \epsilon_{zz} \ \gamma_{xy}]^T$ , where  $\gamma_{xy} = \epsilon_{xy} + \epsilon_{yx}$ , follows from the displacement vector as  $[\epsilon] = [L][u]$ . The effective stress  $[\sigma'] = [\sigma'_{xx} \ \sigma'_{yy} \ \sigma'_{zz} \ \sigma'_{xy}]^T$  follows from the stiffness matrix and the strain vector as  $[\sigma'] = -[D][\epsilon]$ . The fourth order material stiffness tensor is mapped on a simple matrix and reads

$$[D] = \begin{bmatrix} K + \frac{4}{3}G & K - \frac{2}{3}G & K - \frac{2}{3}G & 0 \\ K - \frac{2}{3}G & K + \frac{4}{3}G & K - \frac{2}{3}G & 0 \\ K - \frac{2}{3}G & K - \frac{2}{3}G & K + \frac{4}{3}G & 0 \\ 0 & 0 & 0 & G \end{bmatrix} \quad (2.22)$$

In this expression  $K$  ( $\text{N/m}^2$ ) denotes the compression or bulk modulus of the soil and  $G$  ( $\text{N/m}^2$ ) is its shear modulus. The bulk modulus and the shear modulus follow from Lamae's constants as  $K = \lambda + \frac{2}{3}\mu$  and  $G = \mu$ . Alternatively the Young's modulus  $E$  ( $\text{N/m}^2$ ) and Poisson's ratio  $\nu$  (-) can be used according to

$$K = \frac{E}{3(1-2\nu)}, \quad G = \frac{E}{2(1+\nu)} \quad (2.23)$$

The storage equation (2.17) written in matrix form reads

$$[m]^T \frac{\partial}{\partial t} [\epsilon] + n\beta \frac{\partial p}{\partial t} = [\nabla]^T \left( \frac{1}{\mu'} [\kappa] ([\nabla]p - \rho' [g]) \right) \quad (2.24)$$

where  $[m]^T [\epsilon] = \epsilon_v$  and  $\epsilon_v = \epsilon_{xx} + \epsilon_{yy}$ . The compressibility of the fluid phase corresponds to the inverse of the liquid phase compression modulus  $K^l$  ( $\text{N/m}^2$ ) as  $\beta = 1/K^l$ . The intrinsic permeability is expressed by its matrix as

$$[\kappa] = \begin{bmatrix} \kappa_{xx} & 0 \\ 0 & \kappa_{yy} \end{bmatrix} \quad (2.25)$$

The governing equations (2.21) and (2.24) will be closed by deformation boundary conditions (2.8) and (2.9) in combination with flow boundary conditions (2.18) and (2.19).



### 3 Numerical model

The primary field variable in the equilibrium equation is the soil displacement and the primary variable in the storage equation is the pore pressure. Nodal approximations will be written as  $[u]^T = [u_{x1} u_{y1} \dots u_{xn} u_{yn}]$  and  $[p]^T = [p_1 \dots p_{n_n}]$ , where  $n_n$  denotes the number of nodes. The finite element method imposes a trial function for both that can be written as

$$\hat{u} = [A][u], \quad \hat{p} = [N][p] \quad (3.1)$$

where  $[A]$  (-) is the dimensional extended basis function matrix  $[N]$  (-) given by

$$[A^i] = \begin{bmatrix} N_i^u & 0 & 0 \\ 0 & N_i^u & 0 \\ 0 & 0 & N_i^u \end{bmatrix}, \quad [N] = [N_1^p \quad N_2^p \quad \dots \quad N_{n_n}^p] \quad (3.2)$$

Here  $N_i$  (-) denotes a single basis function and the column  $[A^i]$  adds to the extended basis function matrix as  $[A] = [ [A^1] [A^2] \dots [A^{n_n}] ]$ . Strain state variables follow from

$$\epsilon = [B][u], \quad q = -\frac{1}{\mu'} [\kappa] ([\nabla N][p] + \rho^l [g]) \quad (3.3)$$

where  $[B]$  (1/m) denotes the basis function spatial derivatives matrix that extends  $[\nabla N]$  (1/m). Spatial derivatives of the basis function relate to the strain interpolation matrix  $[B^i] = [LN_i]$ . These matrices are given by

$$[B^i] = \begin{bmatrix} \frac{\partial N_i^u}{\partial x} & 0 & 0 \\ 0 & \frac{\partial N_i^u}{\partial y} & 0 \\ 0 & 0 & \frac{\partial N_i^u}{\partial z} \\ \frac{\partial N_i^u}{\partial y} & \frac{\partial N_i^u}{\partial x} & 0 \end{bmatrix}, \quad [\nabla N] = \begin{bmatrix} \frac{\partial N_1^p}{\partial x} & \frac{\partial N_2^p}{\partial x} & \dots & \frac{\partial N_{n_n}^p}{\partial x} \\ \frac{\partial N_1^p}{\partial y} & \frac{\partial N_2^p}{\partial y} & \dots & \frac{\partial N_{n_n}^p}{\partial y} \end{bmatrix} \quad (3.4)$$

The extended matrix follows from its components as  $[B] = [ [B^1] [B^2] \dots [B^{n_n}] ]$ .

#### 3.1 Numerical formulation

The weak form of the equilibrium equation (2.21) reads

$$\int_{\Omega} [A]^T [L]^T [\hat{\sigma}] d\Omega - \int_{\Omega} [A]^T \rho [g] d\Omega = [0] \quad (3.5)$$

Application of Green's theorem and imposing Cauchy boundary conditions (2.9) gives

$$\int_{\Omega} [B]^T [\hat{\sigma}] d\Omega = - \int_{\Omega} [A]^T \rho [g] d\Omega + \int_{\Gamma_2^u} [A]^T [\bar{\tau}] d\Gamma \quad (3.6)$$

and its incremental form reads

$$\int_{\Omega} [B]^T [\Delta \hat{\sigma}] d\Omega = - \int_{\Omega} [A]^T \Delta \rho [g] d\Omega + \int_{\Gamma_2^u} [A]^T [\Delta \bar{\tau}] d\Gamma + [R^i] \quad (3.7)$$

where the residual is given by

$$[R^i] = - \int_{\Omega} [A]^T \rho^i [g] d\Omega + \int_{\Gamma_2^u} [A]^T [\bar{\tau}^i] d\Gamma - \int_{\Omega} [B]^T [\hat{\sigma}^i] d\Omega \quad (3.8)$$

The actual Cauchy stress at the new state  $[\sigma^{i+1}]$ , follows from the previous stress state and incremental stresses as  $[\sigma^{i+1}] = [\sigma^i] + [\Delta \sigma]$ . The residual was calculated for the previous time step and should be zero approximately.

$$\begin{aligned} - \int_{\Omega} [B]^T [D][L][\Delta \hat{u}] d\Omega + \int_{\Omega} [B]^T \Delta \hat{p}[m] d\Omega = \\ - \int_{\Omega} [A]^T \Delta \rho [g] d\Omega + \int_{\Gamma_2^u} [A]^T [\Delta \bar{\tau}] d\Gamma + [R^i] \end{aligned} \quad (3.9)$$

The actual displacement for the new state follow from the previous state of the system and the incremental displacement as  $[u^{i+1}] = [u^i] + [\Delta u]$ . The Galerkin formulation sets equation (3.9) to

$$\begin{aligned} - \int_{\Omega} [B]^T [D][B][\Delta u] d\Omega + \int_{\Omega} [B]^T [m][N][\Delta p] d\Omega = \\ - \int_{\Omega} [A]^T \Delta \rho [g] d\Omega + \int_{\Gamma_2^u} [A]^T [\Delta \bar{\tau}] d\Gamma + [R^i] \end{aligned} \quad (3.10)$$

The internal force vector of the residual vector given by equation (3.8) for the previous follows from

$$[\sigma^n] = - [D][B][u^n] + [m][N][p^n] \quad (3.11)$$

The weak form of the storage equation (2.24) follows from

$$\begin{aligned} \int_{\Omega} [N]^T [m]^T \frac{\partial}{\partial t} [\hat{\epsilon}] d\Omega + \int_{\Omega} n\beta [N]^T \frac{\partial \hat{p}}{\partial t} d\Omega = \\ \int_{\Omega} [N]^T [\nabla]^T \left( \frac{1}{\mu'} [\kappa] ([\nabla] p - \rho^l [g]) \right) d\Omega \end{aligned} \quad (3.12)$$

Green's theorem applied to equation (3.12) and imposing Neumann boundary conditions (2.19) then gives

$$\begin{aligned} \int_{\Omega} [N]^T [m]^T \frac{\partial}{\partial t} [\hat{\epsilon}] d\Omega + \int_{\Omega} n\beta [N]^T \frac{\partial \hat{p}}{\partial t} d\Omega = \\ - \int_{\Omega} \frac{1}{\mu'} [\nabla N]^T [\kappa] ([\nabla] \hat{p} - \rho' [g]) d\Omega + \int_{\Gamma_2^p} [N]^T [\bar{q}_n^{i+1}] d\Gamma \end{aligned} \quad (3.13)$$

Galerkin weighting and substitution of the interpolation functions then gives

$$\begin{aligned} \int_{\Omega} [N]^T [m]^T [B] \left[ \frac{du}{dt} \right] d\Omega + \int_{\Omega} n\beta [N]^T [N] \left[ \frac{dp}{dt} \right] d\Omega = \\ \int_{\Gamma_2^p} [N]^T [\bar{q}_n^{i+1}] d\Gamma - \int_{\Omega} \frac{1}{\mu'} [\nabla N]^T [\kappa] [\nabla N] [p] d\Omega + \int_{\Omega} \frac{\rho'}{\mu'} [\nabla N]^T [\kappa] [g] d\Omega \end{aligned} \quad (3.14)$$

Implicit linear integration in time provides a set of algebraic equations that is written as

$$\begin{aligned} \int_{\Omega} [N]^T [m]^T [B] [\Delta u] d\Omega + \int_{\Omega} n\beta [N]^T [N] [\Delta p] d\Omega \\ + \Delta t \int_{\Omega} \frac{1}{\mu'} [\nabla N]^T [\kappa] [\nabla N] [\Delta p] d\Omega = \Delta t \int_{\Gamma_2^p} [N]^T \Delta [\bar{q}_n] d\Gamma + \Delta t \int_{\Gamma_2^p} [N]^T [\bar{q}_n^i] d\Gamma \\ - \Delta t \int_{\Omega} \frac{1}{\mu'} [\nabla N]^T [\kappa] [\nabla N] [p^i] d\Omega + \Delta t \int_{\Omega} \frac{\rho'}{\mu'} [\nabla N]^T [\kappa] [g] d\Omega \end{aligned} \quad (3.15)$$

Equation (3.10) and equation (3.15) provide two sets of algebraic equations that need to be solved numerically.

### 3.2 Algebraic equations

The set of algebraic equations that follows from a fully coupled equilibrium-storage formulation, the proposed finite element discretization and implicit time integration is written as

$$\begin{bmatrix} -[K] & [Q] \\ [Q]^T & \Delta t [H] + [M] \end{bmatrix} \begin{bmatrix} [\Delta u] \\ [\Delta p] \end{bmatrix} = \begin{bmatrix} 0 & 0 \\ 0 & -\Delta t [H] \end{bmatrix} \begin{bmatrix} [u^i] \\ [p^i] \end{bmatrix} + \begin{bmatrix} [\Delta F] \\ [\Delta V] \end{bmatrix} \quad (3.16)$$

Here  $[H]$  ( $\text{m}^4/\text{Ns}$ ) is the conductivity matrix,  $[K]$  ( $\text{N}/\text{m}^2$ ) denotes the stiffness matrix,  $[Q]$  ( $\text{m}$ ) is the coupling matrix,  $[M]$  ( $\text{m}^4/\text{N}$ ) expresses the compressibility matrix,  $[\Delta F]$  ( $\text{N}/\text{m}$ ) denotes the load column and  $[\Delta V]$  ( $\text{m}^2$ ) is the hydraulic load column. The stiffness matrix follows from

$$[K] = \int_{\Omega} [B]^T [D] [B] d\Omega \quad (3.17)$$

the coupling matrix reads

$$[Q] = \int_{\Omega} [B]^T [m][N] d\Omega \quad (3.18)$$

the compressibility matrix is written as

$$[M] = \int_{\Omega} n\beta [N]^T [N] d\Omega \quad (3.19)$$

and the conductivity matrix reads

$$[H] = \int_{\Omega} \frac{1}{\mu'} [\nabla N]^T [\kappa][\nabla N] d\Omega \quad (3.20)$$

The body force and boundary traction column is given by

$$[\Delta F] = \int_{\Gamma_2^q} [A]^T [\Delta \bar{\tau}] d\Gamma - \int_{\Omega} [A]^T \Delta \rho [g] d\Omega \quad (3.21)$$

and the gravitation force and boundary flux-volume increment reads

$$[\Delta V] = \Delta t \int_{\Omega} \frac{\rho'}{\mu'} [\nabla N]^T [\kappa][g] d\Omega + \Delta t \int_{\Gamma_2^p} [N]^T [\Delta \bar{q}_n] d\Gamma \quad (3.22)$$

The set of algebraic equations (3.16) has to be solved per time step. The actual pore pressure at the new state follows from the previous stress state and the incremental pressure as  $[p^{i+1}] = [p^i] + [\Delta p]$ . The actual displacement follows from  $[u^{i+1}] = [u^i] + [\Delta u]$ . For a non-linear problem Picard iterations resolve the non-linearities and convergence follows from a residual vector norm given by equation (3.16) where the internal force given by equation (3.11) has to balance the external force. The linear problem is solved by a direct solver.



## 4 Numerical experiments

This chapter presents simulation results for a number of oedometer tests and three loading cases: undrained loading, drained loading and hydraulic loading. The vertical boundaries of the sample are closed for flow and a zero displacement in horizontal direction is imposed for all oedometer tests. At the bottom of the sample the boundary condition specifies a zero displacement in both vertical and horizontal directions. At the top and the bottom of the sample a drained condition applies, here the pressure is prescribed. Table 4.1 gathers the material parameters that will be used for simulation.

| variable                           | value                                      |
|------------------------------------|--|
| Young's modulus $E_{oed}$          | $10^7 \text{ N/m}^2$                       |
| Poisson's ration $\nu$             | 0  |
| porosity $n$                       | 0.33                                       |
| wet soil weight $\gamma^s$         | $2 \cdot 10^4 \text{ N/m}^3$               |
| pore fluid weight $\gamma^l$       | $10^4 \text{ N/m}^3$                       |
| pore fluid compressibility $\beta$ | $6.122 \cdot 10^{-9} \text{ m}^2/\text{N}$ |
| intrinsic permeability $\kappa$    | $1.157 \cdot 10^{-17} \text{ m}^2$         |
| gravitational acceleration $g_y$   | $10.0 \text{ m/s}^2$                       |

Table 4.1 external material parameters

From these values the following parameters can be derived: the bulk modulus of the skeleton  $K$  equals  $3.33 \cdot 10^6 \text{ N/m}^2$ , the shear modulus of the soil  $G$  is  $5 \cdot 10^6 \text{ N/m}^2$ , the hydraulic conductivity  $k$  is  $10^{-5} \text{ m/d}$ , and the void ratio  $e$  equals 0.4925. The compression modulus of the water phase  $K^l$  is  $1.633 \cdot 10^8 \text{ N/m}^2$  and followed from  $K^l = 3nK(\nu_u - \nu) / [(1 - 2\nu_u)(1 + \nu)]$ , where the undrained Poisson ratio  $\nu_u$  was set to 0.495. The compressibility of the soil  $\alpha$  or  $m_v$  equals  $10^{-7} \text{ m}^2/\text{N}$  and the compressibility of the liquid phase  $\beta$  equals  $6.122 \cdot 10^{-9} \text{ m}^2/\text{N}$ . The compressibility coefficients follow from  $\alpha = 1/K + \frac{4}{3}G$  and  $\beta = 1/K^l$ . The consolidation coefficient  $c_v$  then reads  $1.157 \cdot 10^{-7} \text{ m}^2/\text{s}$  as  $c_v = k / [\rho^l g (\alpha + n\beta)]$ .

### 4.1 Undrained loading

The section presents the undrained loading case. Dissipation of water pressure for a one-dimensional consolidation problem [8] follows from

$$\frac{\partial p}{\partial t} = c_v \frac{\partial^2 p}{\partial y^2} \quad (4.1)$$

The analytical solution for this one-dimensional consolidation equation (4.1) for the case where  $p = 0$  for  $y = 0$  and  $p = 0$  for  $y = 2h$  [7] reads

$$\frac{p(t)}{p_0} = \frac{4}{\pi} \sum_{j=1}^{\infty} \frac{(-1)^{j-1}}{2j-1} \cos \left[ (2j-1) \frac{\pi}{2} \left( \frac{h-y}{h} \right) \right] \exp \left[ -(2j-1)^2 \frac{\pi^2}{4} \frac{c_v t}{h^2} \right] \quad (4.2)$$

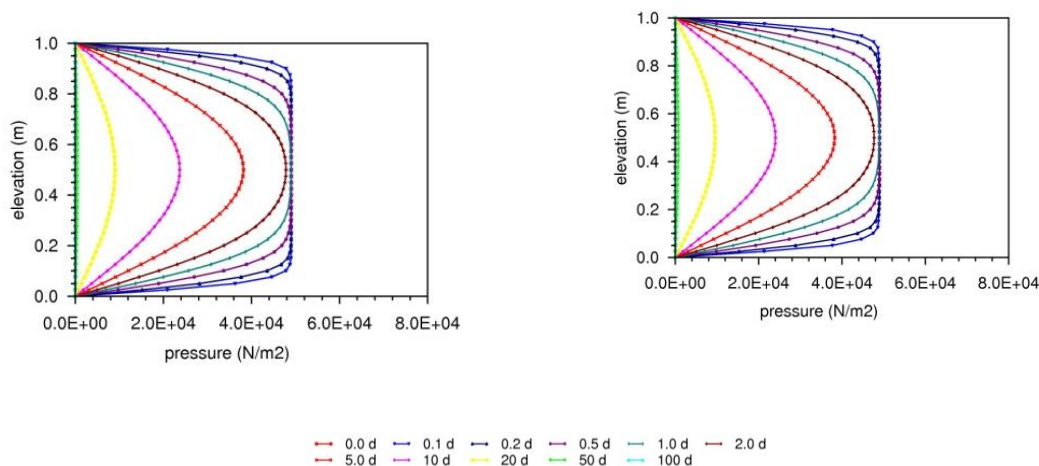


Figure 4.1 Numerical and closed form solution for undrained loading.

Undrained mechanical loading applies a compressive force  $\tau = 50 \text{ kN/m}^2$  at the top of the soil column. Bottom and top are drained and a pressure  $p = 0 \text{ kN/m}^2$  applies. Figure 4.1 compares the numerical solution and the closed form solution for undrained loading. Results compare well.

Figure 4.2 gives the results for the undrained loading presided by gravity loading. A pressure  $p = 0 \text{ kN/m}^2$  applies at the top and  $p = 10 \text{ kN/m}^2$  applies at the bottom. These conditions produce a hydrostatic pressure distribution at the end of the simulation for which the pore water does not flow. Gravity loading gives a total stress  $\sigma = 0 \text{ kN/m}^2$  at the top and  $\sigma = 20 \text{ kN/m}^2$  at the bottom as the soil density equals  $20 \text{ kN/m}^3$ . For the initial situation displacements are set to zero. Mechanical loading generates water pressures and hardly increases effective stresses at the beginning of the process. Total stresses do increase as these stresses sum the pore water pressure and the effective stress. The total stress  $\sigma = 50 \text{ kN/m}^2$  at the top and  $\sigma = 70 \text{ kN/m}^2$  at the bottom due to loading. The load distribution corresponds to equation (1.3). In time water pressures dissipate and the increase in effective stress resembles the loading force per surface area. The final displacement follows Hook's law for a linear material.

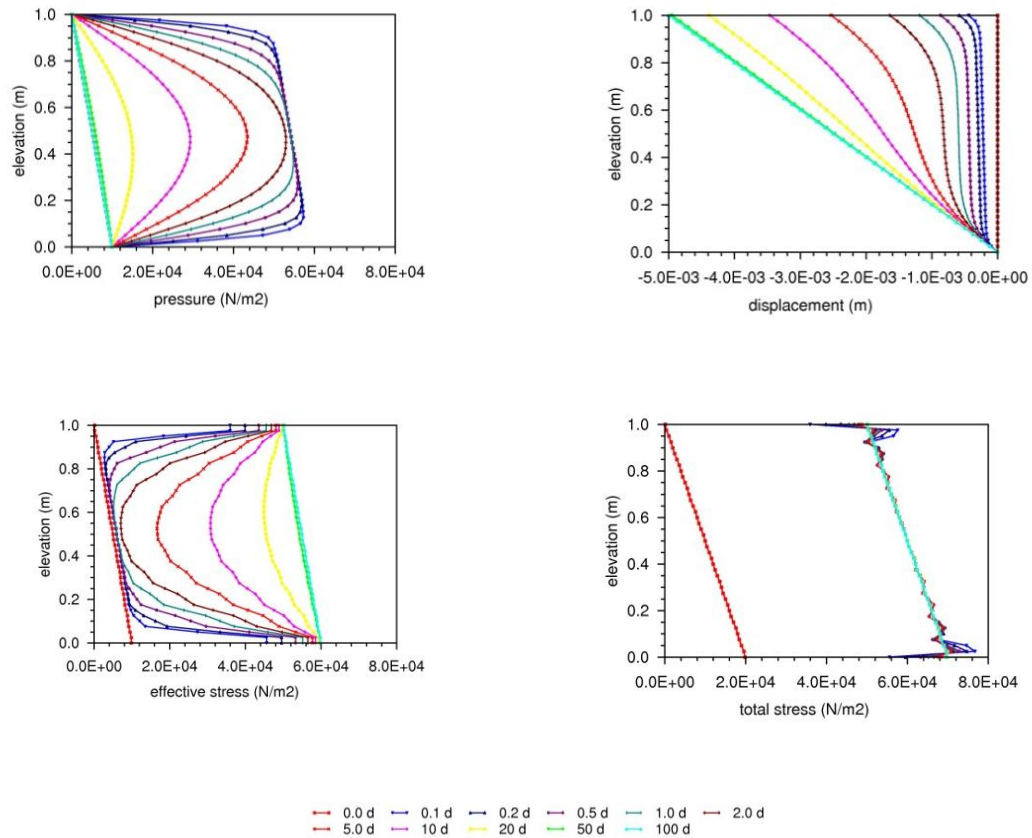


Figure 4.2 Undrained loading presided by gravity loading

The algorithm performed well in simulating the oedometer tests, however the results show pressure oscillations. A combination of six-node triangular elements for displacements and three-node triangular elements for pressure provides consistent stresses in the integration points. The higher order elements need to be sub-parametric; the low order elements remain iso-parametric. The number of integration point needed has to be examined as well as the graphical procedure that extrapolates stresses at the integration points to nodal points. The pressure oscillation may also be a result of mesh orientation effects. The pressure oscillations need further investigation.

## 4.2 Drained loading

This section presents the drained loading case. The load function is given by

$$\tau_c = \begin{cases} \tau^0 + (\tau^1 - \tau^0)t/t^1 & \text{if } t < t^1 \\ \tau^1 & \text{if } t \geq t^1 \end{cases} \quad (4.3)$$

where the mechanical condition at the top is given by a prescribed compressive force. The mathematical formulation of the boundary conditions is supported by  $t^1 = 1$  d,  $\tau^0 = 0$  kN/m<sup>2</sup>, and  $\tau^1 = 50$  kN/m<sup>2</sup>. Figure 4.3 shows the results for the drained loading case.

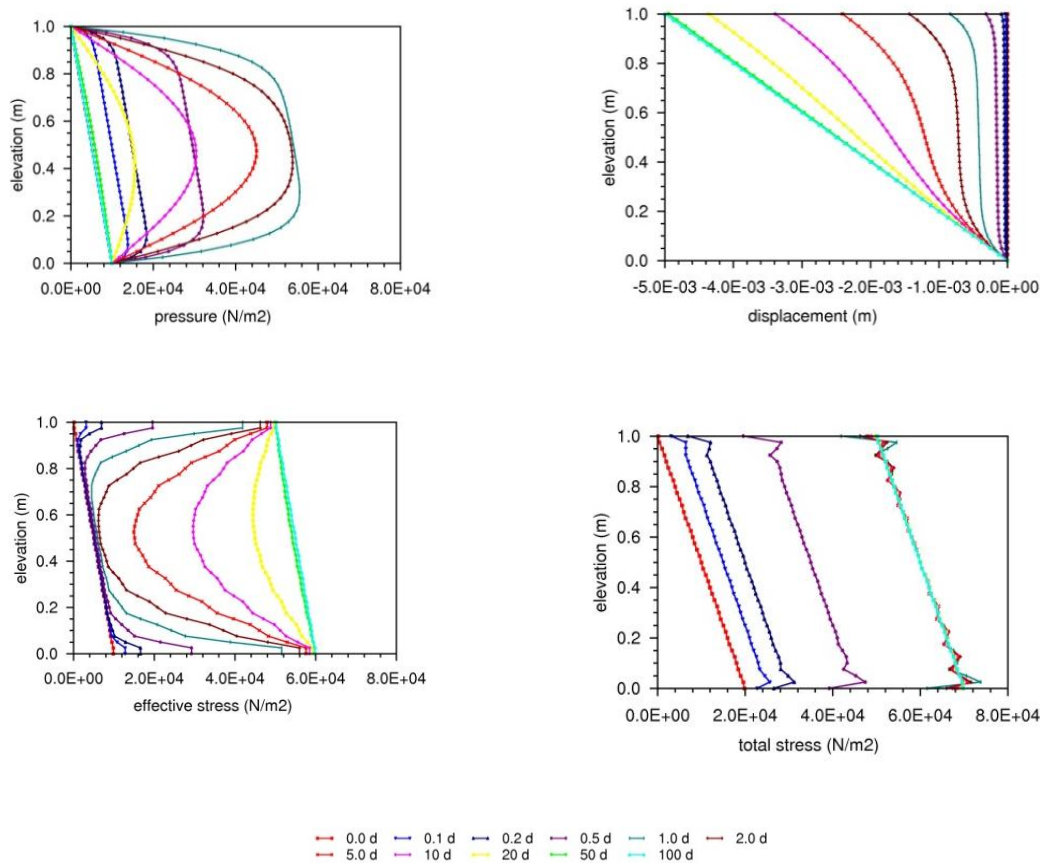


Figure 4.3 Drained loading.

### 4.3 Hydraulic loading

This section presents the hydraulic loading case. The pressure loading follows from

$$p_c = \begin{cases} p^0 + (p^1 - p^0)t/t^1 & \text{if } t < t^1 \\ p^1 & \text{if } t \geq t^1 \end{cases} \quad (4.4)$$

Hydraulic loading sets a time depended water table to the top of the soil sample, water pressures at the bottom remain constant. As a result of these boundary conditions groundwater flow occurs in downward direction and increases in time until a steady state situation is established. A linear water head rise of five meters in one day at the top is translated in loading case parameters:  $t^1 = 1$  d,  $p^0 = 0$  kN/m<sup>2</sup>, and  $p^1 = 50$  kN/m<sup>2</sup>. At the bottom of the soil sample  $p = 10$  kN/m<sup>2</sup>. Maximum displacements are found for the steady state situation. The linear pressure distribution corresponds to a nonlinear displacement distribution.

Figure 4.4 shows the results for the hydraulic loading case.

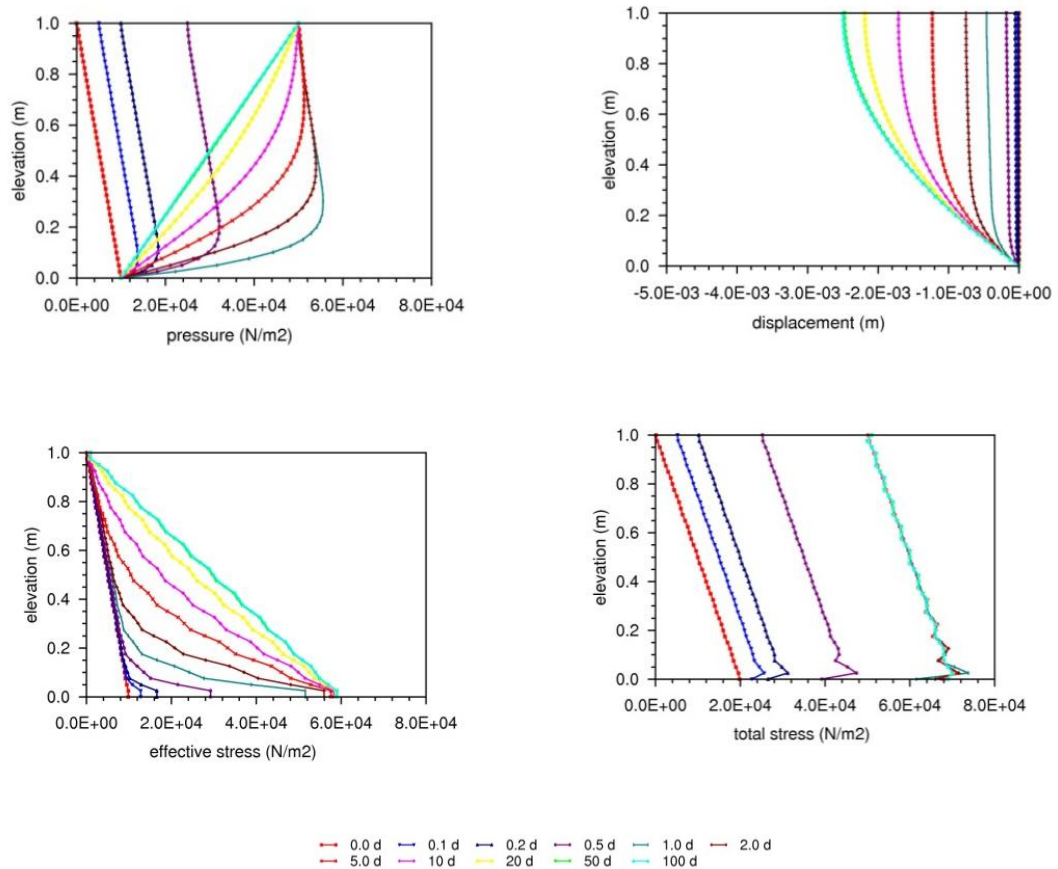


Figure 4.4 Hydraulic loading.



## 5 Conclusions

In general, modeling transient groundwater flow will provide less conservative pore water pressure fields for the stability assessment of dikes than steady state simulations. Nowadays these pore water fields follow from solving the storage equation. This procedure provides a computational efficient method and requires less soil parameters than solving Biot's problem. However the storage equation is not able to simulate the generation of pore water pressure due to hydraulic loading and compression of the subsurface. The Biot model couples the storage equation to the equilibrium equation and is able to simulate the generation and dissipation process.

This report presents a numerical model for solving Biot's problem that considers pore water pressures and displacement of the soil. The numerical code is added to the Deltares groundwater flow module (DgFlow) which supports the dike analysis module (DAM) of the flood early warning system (FEWS). The model applies for plane strain quasi-static fully coupled flow - deformation problems and is able to simulate groundwater pressure generation and dissipation as a consequence of loading the subsurface. Six-node triangular finite elements discretize the equilibrium equation and three-node triangular elements discretize the storage equation. A fully implicit finite difference scheme integrates the ordinary differential equations in time. The numerical examples considered in this report, impose linear elastic soil behavior, which gives rise to a linear set of algebraic equations that was resolved by a direct solver per time step. Numerical simulations have to show the consequences of neglecting the deformations in the prediction of transient groundwater pressure fields in both ways. The flow-deformation formulation simulates pore pressures and soil displacements that can both be monitored in the field.

The algorithm was used to simulate a set of oedometer tests and performed well, however the results show pressure oscillations. A combination of six-node triangular elements for displacements and three-node triangular elements for pressure provides consistent stresses in the integration points. The higher order elements need to be sub-parametric; the low order elements remain iso-parametric. The number of integration point needed has to be examined as well as the procedure that extrapolates stresses at the integration points to nodal points in order to provide graphical results. The pressure oscillation may also be a result of mesh orientation effects.

Future work should include verification tests based on analytic solutions and more complex Plaxis simulations. A comparison with Watex simulation results should also be made, which could support the use of the newly developed DgFlow algorithm. Validation tests could demonstrate the applicability of the model and a parameter study should indicate for which cases the generation of pore water pressures should be included in modeling transient groundwater flow for stability assessment. Future work should also consider the applicability of the heuristic loading procedure already implemented in Fews-Dam.

Figure 5.1 shows the proposed finite element mesh for solving the coupled flow-deformation problem. This setup will be used in order to compare the DgFlow with Watex and Plaxis.

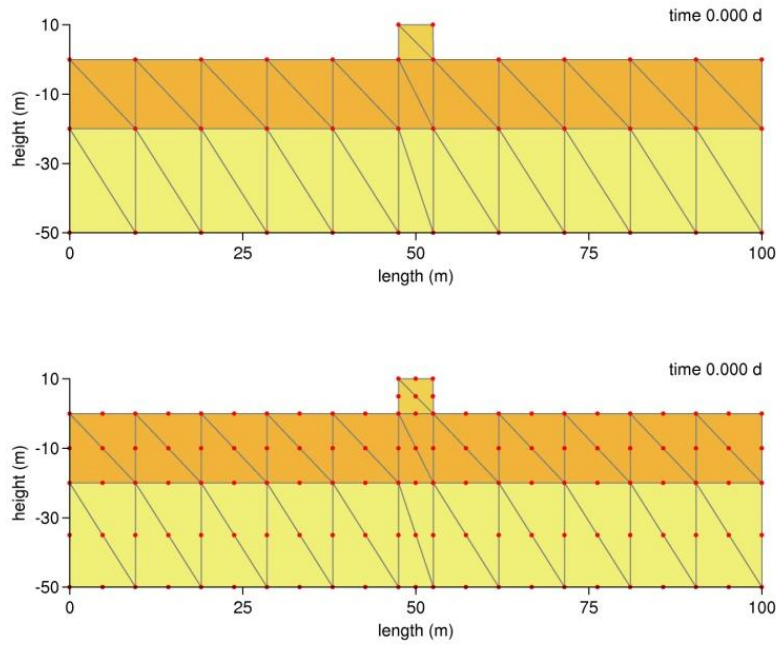


Figure 5.1 Finite element mesh flow-deformation problem.



## Notations

|             |   |
|-------------|---|
| $[A]$       | extended basis function matrix (1/m)                        |
| $[B]$       | basis function spatial derivatives matrix (-)               |
| $c_v$       | consolidation coefficient ( $\text{m}^2/\text{s}$ )         |
| $D_{ijkl}$  | material stiffness tensor ( $\text{N}/\text{m}^2$ )         |
| $e$         | void ratio (-)  |
| $E$         | Young's modulus ( $\text{N}/\text{m}^2$ )                   |
| $[F]$       | load column ( $\text{N}/\text{m}$ )                         |
| $g_i$       | gravitational acceleration vector ( $\text{m}/\text{s}^2$ ) |
| $G$         | shear modulus ( $\text{N}/\text{m}^2$ )                     |
| $h$         | river water level (m)                                       |
| $[H]$       | conductivity matrix ( $\text{m}^4/\text{Ns}$ )              |
| $k_r$       | relative permeability (-)                                   |
| $K^l$       | liquid phase bulk modulus ( $\text{N}/\text{m}^2$ )         |
| $[K]$       | elastic stiffness matrix ( $\text{N}/\text{m}^2$ )          |
| $K$         | compression or bulk modulus ( $\text{N}/\text{m}^2$ )       |
| $[L]$       | differential operator (1/m)                                 |
| $[m]$       | stress mapping column (-)                                   |
| $[M]$       | compressibility matrix ( $\text{m}^4/\text{N}$ )            |
| $n$         | porosity (-)  |
| $n_i$       | normal vector (-)   |
| $N$         | basis function (-)  |
| $p$         | pore pressure ( $\text{N}/\text{m}^2$ )                     |
| $q_i$       | Darcy flux vector (m/s)                                     |
| $\bar{q}_n$ | inflow (m/s)  |
| $[Q]$       | coupling matrix (m)   |
| $S$         | saturation (-)  |
| $t$         | time (s)  |
| $v_i$       | liquid phase velocity vector (m/s)                          |
| $w_i$       | solid phase velocity vector (m/s)                           |
| $[V]$       | hydraulic load ( $\text{m}^2$ )                             |
| $x_i$       | space coordinate vector (m)                                 |
| $\alpha$    | soil skeleton compressibility ( $\text{N}/\text{m}^2$ )     |

|                 |  |
|-----------------|--|
| $\beta$         | pore water compressibility ( $\text{N/m}^2$ )  |
| $\Gamma$        | deformation-flow boundary (m)                  |
| $\delta_{ij}$   | Kronecker delta (-)                            |
| $\epsilon_{ij}$ | strain tensor (-)                              |
| $\epsilon_v$    | volumetric strain (-)                          |
| $\kappa_{ij}$   | intrinsic permeability tensor ( $\text{m}^2$ ) |
| $\lambda$       | Lam\{e\} constant ( $\text{N/m}^2$ )           |
| $\mu$           | Lam\{e\} constant ( $\text{N/m}^2$ )           |
| $\mu^l$         | dynamic viscosity (kg/ms)                      |
| $\nu$           | Poisson's ratio (-)                            |
| $\nu_u$         | Poisson's ratio undrained (-)                  |
| $\rho$          | soil density ( $\text{kg/m}^3$ )               |
| $\rho^s$        | solid phase density ( $\text{kg/m}^3$ )        |
| $\rho^l$        | liquid phase density ( $\text{kg/m}^3$ )       |
| $\sigma_{ij}$   | total Cauchy stress tensor ( $\text{N/m}^2$ )  |
| $\sigma'_{ij}$  | effective stress tensor ( $\text{N/m}^2$ )     |
| $\bar{\tau}_i$  | boundary compression force vector (N/m)        |
| $\phi$          | hydraulic head (m)                             |
| $\Omega$        | deformation-flow domain ( $\text{m}^2$ )       |
| $[\nabla]$      | gradient operator (1/m)                        |

## Bibliography

- 1) R.B.J. Brinkgreve. Plaxis, Finite Element Code for Soil and Rock Analyses. Plaxis B.V., Delft, The Netherlands, 8th edition, 2002.
- 2) R.B.J. Brinkgreve, R. Al-Khoury, and J.M. van Esch. Plaxflow. Plaxis B.V., Delft, The Netherlands, 1th edition, 2003.
- 3) J.M. van Esch. Adaptive Multiscale Finite Element Method for Subsurface Flow Simulation. PhD thesis, Delft University of Technology, Delft, The Netherlands, 2010.
- 4) J.M. van Esch. Modeling groundwater flow through dikes for real time stability assessment. In Computational Water Resources Research, 2012.
- 5) J.M. van Esch. Modeling groundwater flow through embankments for climate change assessment. In Computational Water Resources Research, 2012.
- 6) J.M. van Esch and J.B. Sellmeijer. Modeling transient groundwater flow and piping under dikes and dams. In G.N. Pande and S. Pietruszczak, editors, Computational Geomechanics (ComGeo III). Taylor & Francis Group, 2013.
- 7) A. Verruijt. Grondmechanica. Delftse Uitgevers Maatschappij, Delft, The Netherlands, 1990.
- 8) A. Verruijt. Computational Geomechanics, volume 7 of Theory and Applications of Transport in Porous Media. Kluwer Academic Publishers, 1995.
- 9) A.H. Weerts, J. Schellekens, and F.S. Weiland. Real-time geospatial data handling and forecasting: Examples from delft-fews forecasting platform/system. Journal of Selected Topics in Applied Earth Observations and Remote Sensing, 3(3):386–394, 2010.